Available online at www.sciencedirect.com
SCIENCE DIRECT®
Journal of Electroanalytical Chemistry 584 (2005) 54–62
Journal of Electroanalytical Chemistry
www.elsevier.com/locate/jelechem

Non uniformities of silicon oxide films grown in peroxide mixtures

V. Bertagna [a,*], S. Petitdidier [b], N. Rochat [b], D. Rouchon [b], P. Besson [c], R. Erre [a], M. Chemla [d]

[a] Department of Materials Chemistry, CRMD, CNRS-Université d'Orléans, Rue de Chartres, BP 6759, 45067 Orléans, France
[b] STMicroelectronics, 850 rue Jean Monnet, 38926 Crolles Cedex, France
[c] CEA/LETI, CEA-Grenoble, 17 rue des martyrs, 38054 Grenoble Cedex 9, France
[d] LI2C, Université P. & M. Curie, 4 place Jussieu, 75005 Paris, France

Received 18 May 2004; received in revised form 23 September 2004; accepted 8 October 2004
Available online 30 December 2004

Abstract

The growth kinetics of silicon chemical oxides in H_2O_2-containing solutions at various pH values and temperatures was studied by electrochemical impedance spectroscopy (EIS), ellipsometry and X-ray photoelectron spectroscopy (XPS). Infrared (IR) spectroscopy was also used to investigate the evolution of the surface chemistry from the initial Si–H hydrogen coverage to the subsequent oxidation states by analysing the Si–O–Si stretching vibration modes. Successive EIS diagrams obtained in SC1 solutions ($NH_3 + H_2O_2 + H_2O$) as a function of time constituted a series of semicircles indicating that the semiconductor/oxide/electrolyte (SOE) junction can be modelled as an RC circuit, in which the R term increased to almost 1 $M\Omega\,cm^2$ after 3 h. It is generally known that, in alkaline solutions such as SC1, the oxidation rate rapidly reaches a steady regime controlled by the interfacial charge transfer reaction and the subsequent dissolution of the generated chemical oxide. Accordingly, we propose a mechanism involving a diffusion process of reactants through the oxide barrier followed by a simultaneous dissolution of the layer. Moreover, in acidic media such as SC2 ($HCl + H_2O_2 + H_2O$), even though the solubility is extremely low, we have extended our model based on the competition between the oxidation rate at the surface and the dissolution on the nanoscopic scale of the built-up oxide. Both EIS and IR spectroscopy of the residual Si–H_x bonds lead to a non-uniformity of the surface oxide growth proceeding from island nuclei. In addition, thickness measurements by ellipsometry together with the observed gradual change in the IR spectrum of the Si–O–Si vibration mode were interesting parameters revealing that the oxide growth proceeds simultaneously with an evolution of the structure leading to a more compact and insulating dielectric layer.

Keywords: Silicon oxide; Growth kinetics; Silicon surface treatment; Electrochemical impedance

1. Introduction

The RCA process, originally developed by Kern and Puotinen [1,2], is still widely used in the semiconductor industry for the surface cleaning of silicon wafers. New improvements are continually initiated aiming at a better cleaning efficiency, a lower cost, and a strict control of the environmental regulations [3,4]. After removal of the native oxide with a HF treatment, the resulting hydrophobic surface covered with Si–H_x terminal bonds is successively treated in an alkaline ammonia + hydrogen peroxide mixture called SC1, to oxidize the inorganic contaminants and generate a thin chemical oxide layer, surrounding both the particles and the substrate surface. As a result an identical zeta potential is generated for both interfaces so as to create repulsion forces between the Si surface and the particles. In the next step, an acidic HCl + hydrogen peroxide mixture

* Corresponding author. Tel.: +33 2 38 49 48 65; fax: +33 2 38 41 70 43.
E-mail address: valerie.bertagna@univ-orleans.fr (V. Bertagna).

0022-0728/$ - see front matter © 2004 Elsevier B.V. All rights reserved.
doi:10.1016/j.jelechem.2004.10.028

called SC2 allows the metallic contaminants to be dissolved as complex species and excluded from the surface. The pH value of these solutions is the determining factor to optimise the elimination of contaminants, particles, organic or metallic species [5]. Most of the optimizations implemented nowadays aim at increasing the cleaning efficiency and decreasing the chemical cost and consumption, the time of process and the size of the wet bench in the clean room. As examples, we can quote the use of diluted chemistry and megasonics, and furthermore the introduction of chelating reagents [6]. These treatments lead to a thin chemical silicon oxide layer, before thermal silicon oxide build up.

For the purpose of down-scaling the elemental CMOS (complementary metal oxide semiconductor) components, the thickness of the ultra-thin thermal silicon oxide (12 Å), built upon the chemical oxide, has to be decreased. But, with such a thin insulating layer, the leakage tunneling current becomes a stringent limiting factor [7]. In the next CMOS generation, other dielectric metal oxide materials, called high-k, will supplant the ultra-thin silicon gate oxide. In both cases, the surface preparation step, which is needed to ensure a low interface state density, will generate a chemical oxide playing the role of a transition layer between the substrate and the dielectric stack. The impact of its thickness, structure and composition will be the key parameter for the final high-k multi layer dielectric oxide.

The growth kinetics of a silicon oxide layer from a hydrophobic surface have been already studied in aqueous media in the presence of strong oxidants such as ozone, hydrogen peroxide or dissolved oxygen. Gould and Irene in 1989 [8], investigated by in situ ellipsometry techniques the chemical reactions involved during the aqueous NH_4OH treatment of silicon surfaces.More recently, in alkaline media such as SC1, Adachi and Utani [9] and then Eom et al. [10] reported that the thickness reached a limiting value after a few minutes because of the quasi equilibrium established between the oxidation process and the oxide dissolution. On the other hand, measurements by Ohmi et al. [11] led to the conclusion that, in 30% H_2O_2 at 20 °C, the oxide thickness was initially growing fast and reached a plateau after 1000 min, according to diffusion control of the oxidation process.

The structure of these oxide films has been studied in terms of the remaining Si–H bonds and the position of the Si–O–Si stretching vibration bands by infrared techniques. Ogawa et al. [12] observed that the density of the remaining Si–H surface bonds was 5 times higher in SC2 or HNO_3 than in SC1 or SPM ($H_2SO_4 + H_2O_2$) solution. Using Fourier transform infrared (FTIR) spectroscopy with Si substrate surfaces in contact with a 3% H_2O_2 solution at 20 °C, Sugita and Watanabe [13] detected the coexistence of unoxidized Si–H bonds and oxidized Si–O–Si groups for more than 1000 min. They concluded that the oxidation proceeded through island generation. The use of more than one wet cleaning treatment was also investigated by Ogawa et al. [14] with FTIR attenuated total reflection (FTIR-ATR) spectroscopy and FTIR reflection absorption spectroscopy FTIR-RAS. They concluded that the mechanism involved in SC2 treatment was different from that under other conditions (SPM, SC1, HNO_3) and did not change the properties of the chemical oxide layers formed with other chemicals.

The absorption band due to Si–O–Si groups is composed of two vibrational modes: a longitudinal optical (LO) and a transverse optical (TO) mode [15]. The position of the LO mode has been extensively discussed in the literature as it is sensitive to the structure of the oxide film. Sugita et al. [16] found that the position of the LO mode was dependent on the density of the film measured by X-ray reflection. Moreover, Sugita and Watanabe [13] observed that the position of the LO mode shifted towards higher wave numbers during oxidation in ozone and H_2O_2 aqueous solutions while the Si–H bonds disappeared.

Moreover electrochemical techniques, specifically electrochemical impedance spectroscopy, were used to study in situ the kinetics and interfacial reactivity of the silicon oxide growth in SC1 solutions [17,18]. In these papers we showed, in alkaline media, a higher permeability of the oxide barrier to ions and oxidizing agents, whereas this phenomenon vanished in acidic solutions. This behaviour was assigned to the acido-basic properties of the surface oxide layer, showing the existence of Si–OH bonds, which can be ionized as $Si–O^-$ groups in alkaline media, or alternatively, be transformed into Si–O–Si bonds by bridging in acidic solutions.

In the present work, we report the oxidation process of hydrophobic silicon surfaces in peroxide mixtures, SC1 and SC2, as a function of time, pH and temperature. This study was focused on the reactivity, homogeneity and chemical composition of the growing thin oxide layer.

2. Experimental

All samples were p-type silicon (100) wafers from the production line of STMicroelectronics Co, boron doped ($\approx 10^{15}$ atoms cm^{-3}). They were initially treated with a SPM ($H_2SO_4 + H_2O_2$) solution followed by HF + HCl treatment to obtain a hydrophobic H-terminated surface, following the protocol summarized in Table 1.

Then, the oxidation was studied comparatively in H_2O_2-containing solutions at different pH values and temperatures. The experimental details are listed in Table 2.

Table 1
Summary of the successive steps for sample preparation

Step	Solution	Conditions
Organic removal	SPM	100 cm^3 H_2O_2 in 40 l H_2SO_4 for 5 min
Rinse	DIW (deionized water)	Overflow during 5 min at 50 °C
Native oxide removal and hydrogen passivation	HF:HCl:H_2O	(1:1:100) over 3 min
Rinse	DIW	Overflow over 5 min at 20 °C

Table 2
List of processes used for surface oxidation

Step	Solution	Conditions	Duration (min)
Oxidation	SC1 (NH_3 + H_2O_2 + H_2O)	(1:1:50) at 20 °C	0.4–210
	SC2 (HCl + H_2O_2 + H_2O)	(1:1:50) at 20 and 50 °C	10–290
	H_2O_2 (H_2O_2 + H_2O)	(1:50) at 20 and 50 °C	10–290
Final rinse	DIW	Overflow at 20 °C	10
Dry		Spinning	

Electrochemical experiments were conducted in an electrochemical cell, specially designed to control several parameters, such as the influence of external light and the effect of solution confinement at the seal junction of the sample with the cell [19], so as to optimise the reliability of the results. The back side of the Si sample was kept free from its native oxide and covered with a Ga–In alloy, to obtain an ohmic contact. The cell was connected to an EG & G PAR model 273A potentiostat, and an impedance analyser Solartron 1260. The frequency range was selected from 10 kHz to 0.05 Hz in such a way that a complete impedance diagram was obtained within 2–3 min. This configuration allows the diagrams to be scanned in a short time without noticeable change of the oxide dielectric properties during the data recording. The high frequency region between 10^5 and 10^4 Hz was often not recorded because the inductive component due to the electrical leads could introduce some uncertainty and moreover we observed that the corresponding values did not add to the parameter adjustment of the diagrams. Then the Nyquist plots were modelled in terms of parallel RC loops, whose values were determined using the software Zplot, which is the internal data processor included in the Solartron device. In fact it is known that oxide film|electrolyte interfaces exhibit non-ideal capacitive behaviour, and that a more accurate representation is obtained by substituting the capacitive component of the interfacial impedance $(i\omega C)^{-1}$ by a CPE equal to $Q(i\omega)^{-n}$, where $0 < n < 1$. In this study, the derived n values were very close to 1, except during the very first few minutes of the oxide growth.

The oxide growth kinetics were followed with a Rudolph Fe III ellipsometer with a single wavelength, 632.8 nm, and the thickness was extracted using a refractive index value equal to that of the thermal silicon oxide ($n = 1.462$). We are aware that this value is not very appropriate in the case of very thin chemical oxide layers [20], but the choice of this single index was useful to obtain the relative thickness values of the layer as a function of time. A hydrophobic surface resulting from the HF treatment was the zero reference for the ellipsometric measurements, assuming that the contribution of the Si–H bonds to the optical constant was negligible. To check these values, X-ray photoelectron spectroscopy (XPS) measurements using a spectrometer with an Al Kα X-ray source were performed at two angles, 18° and 35°, on a surface analysis of 250×1000 μm^2. The thickness was determined from the intensity ratio of all the oxidized silicon species detected using the formalism of Yano et al. [21].

On the other hand, our work aimed at the determination of the silicon consumption during the alkaline and acidic chemical treatments. The technique used in this purpose was thickness measurements by ellipsometry, using silicon-on-insulator (SOI) substrates following the procedure described by Celler et al. [22]. The starting wafer consisted of a 2000 Å monocrystalline Si film that was separated by 4000 Å of thermal SiO_2 from the bulk Si substrate. This thermal silicon oxide layer acted as a buried reference layer for the ellipsometric measurements using various wavelengths. The etching rate was derived by measurement of the remaining thickness of the silicon layer after the oxidizing chemical treatment.

The properties of the silicon surface bond vibrations were investigated by FTIR spectroscopy using specific modes depending on the kind of bonds to be detected. The multiple internal reflection (MIR) mode was performed to study the evolution of Si–H_x hydrogen coverage during the oxidation process, because this technique is very sensitive to a few surface sites. The vibration modes corresponding to the Si–H_x surface groups were

obtained by scanning the IR spectrum between 2000 and 2200 cm^{-1}. Attenuated total reflection (ATR) was chosen to detect the evolution of the Si–O–Si and Si–OH vibration spectra, covering the region near 1200 cm^{-1}. Moreover the vibration of the Si–OH bond was observed as a broad band in the interval between 3200 and 3500 cm^{-1}.

3. Results

This experimental investigation started from the results obtained by a series of electrochemical impedance spectroscopy measurements. Successive Nyquist diagrams gave clear indications related to the growth of a silicon oxide insulating layer as a function of time by reaction of the naked surface of a silicon substrate with oxidizing reactants such as SC1 or SC2 solutions. For example the in situ growth kinetics were followed by electrochemical impedance spectroscopy over 3 h at open circuit potential in the dark in SC1 and SC2 solutions. The results are plotted in Fig. 1(a)–(c). The Nyquist plots are semi-circle shaped, and the interface can be modelled as an RC parallel circuit. The capacitance values were found to be equal to a few $\mu F/cm^2$, typical for a SOE (silicon/oxide/electrolyte) junction including the capacitance of an oxide dielectric layer a few Å thick.

Fig. 1(a) depicts the extremely slow impedance variation observed with an initially naked silicon surface, in an acidic SC2 solution. Over 20 h, the diameter of the Nyquist plots increased continually during the silicon oxide growth, so that the resistance reached several $M\Omega\,cm^2$. At room temperature the oxidation mechanism, together with the increase of the resistance proceeded over more than 24 h.

In the case of an alkaline SC1 electrolyte, the surface silicon oxide was formed and the Nyquist plots diameter reached a steady state (Fig. 1(b)) after 3 h duration, indicating a resistance term equal to $\approx 4.5 \times 10^5\ \Omega$, the area of the sample being equal to 3 cm^2. Then, keeping the sample inside the electrochemical cell, the surface was thoroughly rinsed with pure deionized water, and a new SC1 electrolyte was introduced inside the cell, to examine the influence of a possible ageing of the SC1 solution. The shapes of the Nyquist plots obtained were almost superimposed on the preceding ones, indicating that the steady state was, in fact, related to a surface phenomenon. This feature could be, to a first approximation, assigned to the diffusion rate of the oxidizing species through the oxide layer [17]. Moreover, the influence of the solution pH on the same oxide was checked by replacing the SC1 by an SC2 solution. Fig. 1(c) depicts this experiment exhibiting a dramatic increase of the polarization resistance of the interface reaching values as high as several $10^7\ \Omega\,cm^2$. Finally, after a few

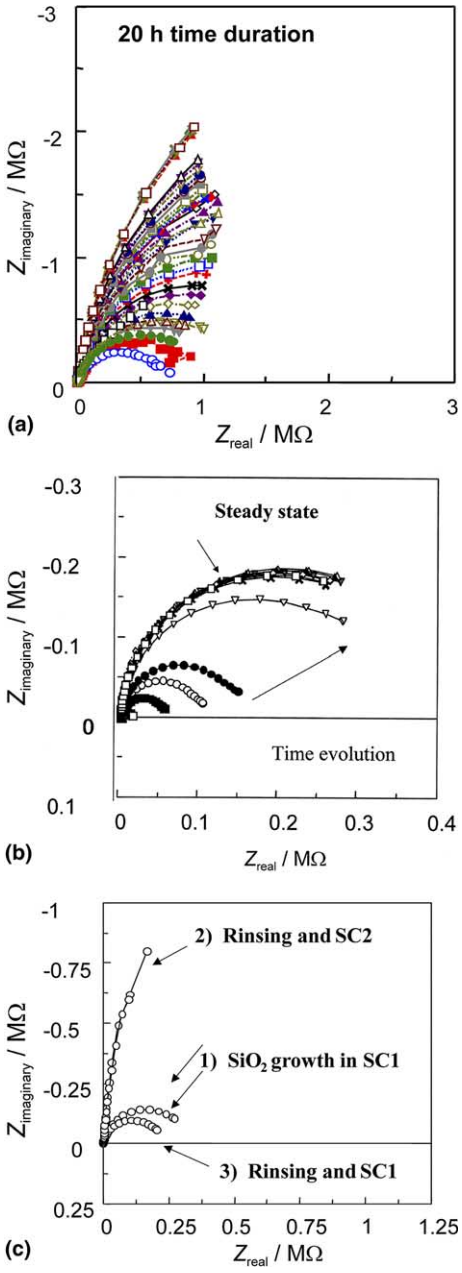

Fig. 1. (a) Successive Nyquist plots recorded on a p-type silicon substrate in a SC2 solution. (b) Successive Nyquist plots recorded on a p-type silicon substrate in a SC1 solution. (c) pH influence of the solution on the electrical parameters of the interface.

minutes, the electrochemical cell was rinsed anew and filled again with SC1 to reproduce the initial experimental conditions. This experiment led to the recovery of the original Nyquist plot obtained in a SC1 solution. We can assume that, during these experiments, the thickness of the chemical silicon oxide did not change significantly. However the polarization resistance value proved to be extremely sensitive to the pH of the electrolyte solution. In acidic solutions the oxide layer is transformed into a more compact insulating layer which

constitutes a tight barrier against electrical and material transport through it. In fact, experiments of oxide growth in acidic SC2 solutions resulted in a series of semicircles as presented in Fig. 1, but the transformation was much slower; the steady state was reached after more than 24 h. We tried to understand these results using other experimental methods.

First, a study of the silicon oxide thickness evolution versus time was carried out on both samples by ellipsometry and XPS. Two distinct types of behaviour for the chemical oxide growth kinetics were evident from ellipsometry as shown in Fig. 2. As previously mentioned, the growth rate was observed to be much more rapid in SC1 solutions [7,8] than in acidic SC2 or neutral H_2O_2 solutions at the same temperature. Even though we do not consider that the thickness data obtained by ellipsometry are not absolute values, we point out that the quasi equilibrium between the oxidation process and the oxide dissolution in SC1 solutions was reached after only a few minutes and led to a limiting thickness of the oxide layer in the vicinity of 5–6 Å at 20 °C. So the continual evolution of the polarization resistance during 3 h cannot be related to a gradual increase of the oxide thickness. These values were very close to those deduced from the XPS data with an oxide thickness of 5.3 and 6.9 Å obtained, respectively, for 7 and 210 min of immersion time.

For this reason an investigation of the oxide layer structure was undertaken using FTIR spectroscopy. Thus it was easily recognized that the faster oxide growth recorded in alkaline SC1 solutions was correlated to a fast removal of the hydrogen Si–H_x surface coverage of the primitive hydrophobic samples after treatment by diluted HF. Fig. 3 shows that this first step of the oxidation process was more effective in SC1 at 20 °C than in SC2 or H_2O_2, even at 50 °C.

On the other hand, the structure of the oxide layer can be depicted more precisely by ATR spectroscopy in the wave number region of 1200 cm^{-1}. In the case of a continuous oxide film, the peak corresponding to the Si–O–Si stretching vibration can be split, according to Berreman [23], into two optical modes: longitudinal (LO, in the vicinity of 1200 cm^{-1}) and transverse (TO, near 1050 cm^{-1}) modes. We recall that for SC1, the thickness is almost immediately higher than one monolayer in correlation with the fast Si–H_x removal rate, and reached a limiting value after a few minutes. Fig. 4 shows that the LO vibration mode appears very early; its intensity increases with time, while the peak shape becomes sharper and its position is gradually shifted to a higher energy vibration mode over 3 h. This result indicates that the oxide layer gradually reaches a more compact and well-defined structure, and is consistent with the observed evolution of the polarization resistance.

Somewhat different behaviour was obtained in acidic SC2 solutions but the evolution rate was extremely slow at room temperature. Thus Fig. 5 shows the successive

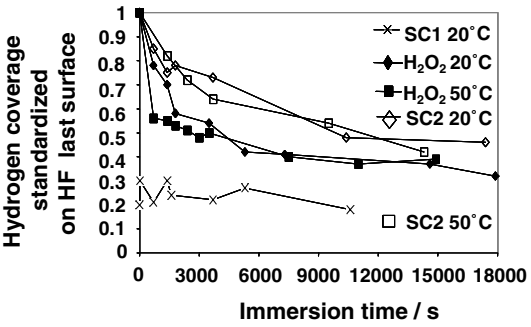

Fig. 3. Time dependence of the Si–H_x hydrogen coverage from MIR spectroscopy versus different process conditions.

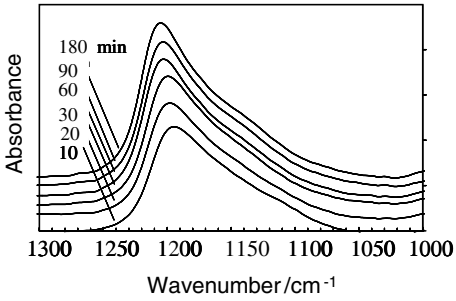

Fig. 4. ATR spectra of the Si–O–Si stretching vibrations in SC1 recorded over 3 h at 20 °C.

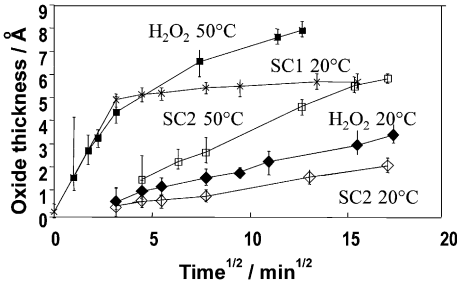

Fig. 2. Optical thickness from ellipsometry versus time plots, for different process conditions.

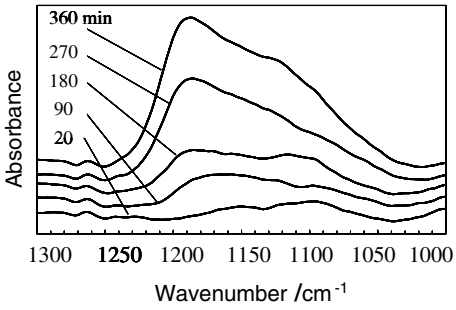

Fig. 5. ATR spectra of the Si–O–Si stretching vibrations in SC2 at 50 °C.

spectra for the Si–O–Si vibration mode obtained at 50 °C. Compared to the results of Fig. 4, the vibration peaks are broader and coarsely defined, indicating a more complex chemical surface composition. In SC2 at 50 °C, the LO mode appears only after 150 min, when the thickness determined by both XPS and ellipsometry reaches 3.1 Å, i.e., when the oxide film is equivalent to about one monolayer, thus indicating that the oxide cannot be considered as a continuous film. These results led us to suggest a non-uniform growth mechanism in SC2, with remaining non-oxidized Si–H_x bonds on the surface. The Si–H_x bonds are extremely stable in acidic media. First, Si–OH groups resulting from the oxidation of Si–H_x bonds appear, yielding the appearance of the TO mode. Subsequently, the Si–Si back bonds linked to the Si–OH groups are predominantly oxidized because of the polarization of these Si–Si bonds induced by the oxygen atoms. Such results are quite consistent with the conclusion of Sugita and Watanabe [13] indicating that the oxide growth proceeded via the primary generation of surface islands. Only after a long immersion time does the growth give rise to an almost uniform oxide film with limited non oxidized regions.

Finally our experiments based on SOI techniques led us to a sound demonstration of the oxidation/dissolution mechanism controlling the surface Si oxide growth. When a silicon oxide is generated in a peroxide mixture, either acidic or basic, a dissolution process occurs at the same time. This phenomenon was quantified on the Å scale using the SOI technique by measurement of the remaining silicon thickness. For example, Fig. 6 depicts the consumed silicon substrate thickness on top of the SOI structure, as a function of various immersion times in a SC1 solution at 20 °C. Although the thickness of the silicon oxide built up on top of the substrate has reached a constant value, the remaining silicon thickness decreased. Considering that the system attained a steady regime of an oxidation/dissolution mechanism, this experiment gives access to the chemical silicon oxide etch rate. This kind of procedure was also carried out with a thick thermal silicon oxide, and led to the results depicted in Fig. 6 which shows that the etch rate of the thermal oxide is below that of the chemically grown oxide. At this stage we recall that the silicon layer constituting the SOI chip was deposited by CVD, and has probably not the same structure as the monocrystalline silicon substrate. Thus the etch rates would be not identical for these two kinds of materials. Table 3 shows quantitative results, related to the silicon etch rate in SC1, SC2 and H_2O_2, obtained using the SOI technique. These experiments demonstrated that the solubility of the oxide (in Å/min) was detectable even in acidic media. It is extremely low, 10 times less, as compared to that for alkaline solutions such as SC1.

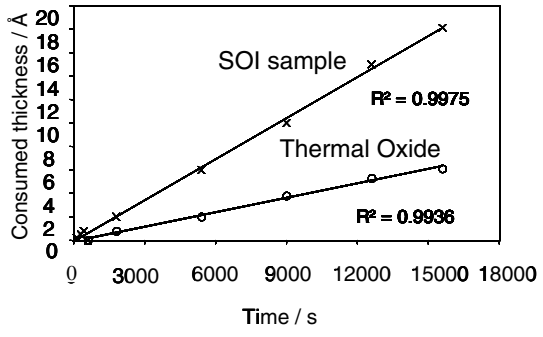

Fig. 6. Consumed silicon oxide thickness versus time measured with the SOI technique.

4. Discussion

From our experimental results, the oxide growth apparently followed a parabolic law in the case of peroxide mixtures with acidic species (SC2) or neutral pH (H_2O_2), since the thickness was approximately linear versus the square root of time (Fig. 2). Nevertheless infra-red spectroscopy results presented in Fig. 3 revealed the survival of terminal Si–H_x bonds for a long time, mainly in the case of acidic (SC2) or neutral (H_2O_2) solutions, and thus demonstrated a non uniform growth mechanism of the surface oxide. The same conclusion holds in the case of SC1 during the initial period preceding the steady regime leading to a plateau. We note that a thickness of less than one monolayer, around 3 Å, is recorded even after 5 h in SC2 at 20 °C, 4 h in H_2O_2 at 20 °C and 1 h in SC2 at 50 °C. The XPS measurements were in a good agreement with these results, indicating a thickness of less than one monolayer. In such acidic solutions and on this scale of time, the oxide growth is extremely slow and the thickness does not reach a plateau, in agreement with the results obtained by Ohmi et al. [11]. We recall that, according to the basic model of oxide growth originally established by Wagner and Grunewald [24], the parabolic law is a result of rate control by diffusion of the reactants through the preexisting layer as well as by field assisted transport of ionic species. This model was later improved by Deal and Grove [25] who introduced additional terms accounting

Table 3
Calculated parameters for the diffusion/reaction model from experimental data processing of the SOI technique

Solution	Temperature (°C)	Silicon etch rate (Å min^{-1})	d_∞ (Å)	$10^{12}D$ (cm^2 s^{-1})
SC1	20	0.09 ± 0.005	5.8	5.9
SC2	20	0.008 ± 0.002	2.5	1.2
	50	0.034 ± 0.004	6.8	3.5
H_2O_2	20	0.005 ± 0.001	7	0.6
	50	0.016 ± 0.003	7.5	7.0

for the presence of an initial oxide layer which leads to the linear-parabolic growth process.

De Smedt et al. [26] have extensively described the field assisted growth of the chemical oxide generated in ozonized water, and concluded that the mechanism could be fitted more closely using the Fehlner formalism [27] than by using the Deal and Grove model [26] based on a pure diffusion phenomenon. They indicate that the diffusion of the reacting species is not the main transport mechanism; a field-assisted drift, where anions can migrate through the oxide film under the influence of an electrical field, should come into play. Due to the oxygen species adsorbed on the silicon surface, a potential drop appears, between the oxidized species and the bulk of the substrate. This potential is constant through the oxide but the electrical field over the oxide layer, calculated as the potential to thickness ratio, can reach extremely high values in the case of ultra-thin insulating layers, which leads to a logarithmic dependence of the thickness versus time. Then, the growth kinetics could be modelled and well represented with the expression (1)

$$d = E\ln(1 + Ft), \tag{1}$$

where E and F are adjusted parameters proportional to the penetration depth of the species and to the concentration of the precursors respectively. In Fig. 7, the experimental thickness of the oxide layers, obtained after SC2 or H_2O_2 treatments, were plotted versus immersion time. Both models, Deal and Grove and Fehlner–Mott were superimposed to the experimental curves. Even though Eq. (1) seems to match the oxide growth kinetics in SC2 and H_2O_2, it was difficult to assign a physical meaning of the adjusted parameters E and F derived from the experimental values. We must point out that generally these models are appropriate to the kinetics of the oxidation mechanism, but none of them accounts for a dissolution process in a liquid phase.

For SC1 solution, we assumed that the growth kinetics were controlled by the diffusion of the species, alternatively by field assisted transport, through the oxide

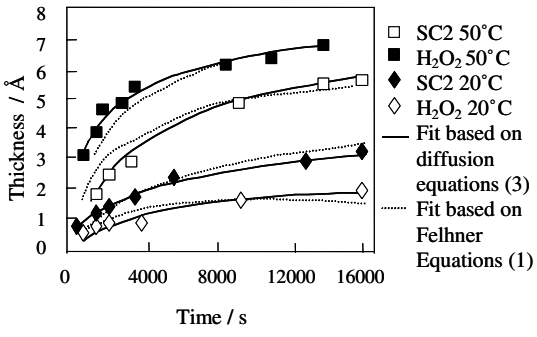

Fig. 7. Comparison of the time dependence between the optical thickness and the fits with the Fehlner or diffusion/dissolution formalism.

layer, but with an additional term K related to the dissolution rate of the oxide [17,18]. This mechanism leads to a parabolic law during the very first stages of the growth, and tends to a plateau corresponding to the steady regime oxidation/dissolution. This can be extended to other peroxide mixtures; the differential equation describing this phenomenon is

$$\partial d/\partial t = D_1 c^0/d - K, \tag{2}$$

where d is the thickness, D_1 is a constant proportional to the diffusion coefficient of the species, c^0 is the concentration of H_2O_2 in the bulk of the solution and K is the constant related to the dissolution rate per surface unit. The integration of Eq. (2), leads to

$$d + (D_1 c^0/K)\ln\{1 - (K/D_1 c^0)d\} = -Kt. \tag{3}$$

It is interesting to check that, at very short times, the development of the logarithmic term to the second order leads to the expected parabolic law

$$d^2 = 2D_1 c^0 t. \tag{4}$$

Eq. (2) also shows that at infinite time, the thickness will reach a limiting value d_∞ corresponding to the quasi equilibrium state of the oxidation/dissolution process

$$d_\infty = D_1 c^0/K. \tag{5}$$

From these equations, the apparent diffusion coefficient D_1, the limiting thickness d_∞, and the corresponding Si substrate etch rate were derived and reported in Table 3. We can see that, as expected, D_1 increases with temperature and pH. As shown in the Fig. 7, the ellipsometric measurements are in line with this model.

In order to interpret the fast oxide growth recorded in SC1, we proposed [17], a purely electrochemical oxidation mechanism, and suggested the following reactions under the zero current conditions for the electron transfer between surface sites and the reactants in solution

$$Si_{(surface)} + 2OH^- \rightarrow Si(OH)_{2(surface)} + 2e^- \tag{6}$$

This generation of electrons is compensated by the simultaneous reduction of hydrogen peroxide

$$H_2O_2 + 2e^- \rightarrow 2OH^- \tag{7}$$

Alternatively, reaction (7) could be written

$$H_2O_2 \rightarrow 2OH^- + 2h^+ \tag{8}$$

These reactions generate Si–OH surface groups, leading to a passive oxide layer with the condensation of hydroxyl bonds. At the same time, the silicon surface oxide is continually refreshed as a consequence of the quasi equilibrium between growth and dissolution. Thus the protecting properties of the oxide passivity is maintained throughout the whole process.

Nevertheless it is worth indicating [17] that in a pure deaerated ammonia solution under zero current condi-

tions, the cathodic reaction concern only the water molecules and results in H_2 evolution or the formation of Si–H bonds. Then reaction (7) should be replaced by

$$Si_{(surface)} + H_2O + e^- \rightarrow Si\text{–}H_{(surface)} + OH^- \quad (9)$$

Such a mechanism leads to the formation of hydrophobic Si–H sites at the interface between the Si substrate and the Si oxide passivating layer, and contributes to loosen its protecting properties, thus leading to the appearance of corrosion pits.

From our experimental results, an additional surface reaction controlling the oxidation rate is the partial acido-basic dissociation process for the generated silanol groups

$$\text{-Si(OH)}_2 \rightarrow \text{-Si}\begin{matrix}\diagup\ \text{OH} \\ \\ \diagdown\ \text{O}^-\end{matrix} + H^+ \quad (10)$$

These ionized chains are highly hydrophilic, thus leading to an easy diffusion of the species, H_2O_2 and H_2O, through the oxide thin film and a higher electrical conductance of the layer. This could be the reason why a steady state regime is established within a rather short time during SC1 treatment.

Nevertheless we can assume that the surface acidity of Si–OH groups is extremely weak, so that the fraction of ionized sites is very small. Indeed, if we recall that the resistance of the 5 Å thick layer is $\approx 1\ M\Omega\ cm^2$, the order of magnitude of this oxide bulk resistivity is a few $10^{13}\ \Omega\ cm$. Subsequently the remaining Si–OH groups will interact together to generate more tightly bound Si–O–Si bridges. This mechanism was clearly supported by the continuous increase of the LO vibration mode of these bonds obtained by ATR spectroscopy. This LO peak becomes sharper with time and is shifted from 1195 to 1205 cm^{-1} as the immersion time increases from 10 to 180 min, indicating a better organization of the oxide film. As a comparison, the frequency of the LO peak for thin thermally oxidized SiO_2 films is in the vicinity of 1250 cm^{-1}. As a conclusion, the continuous evolution over 3 h observed on Nyquist diagrams obtained in alkaline SC1 solutions, cannot be related to an increase of the silicon oxide thickness, but is related to an evolution of the surface chemistry with the condensation of Si–OH species giving rise to a more compact and insulating structure induced by Si–O–Si bridging [28].

Section 2 also showed that the acidification using SC2 solution led to a much more insulating surface oxide layer, because of the neutralization of the negatively charged sites $Si\text{–}O^-$ by protons, and followed by the condensation of neutral $Si(OH)_2$ into more tightly bound Si–O–Si bridges. This behaviour is responsible for the sudden increase of the polarization resistance value, which was observed by electrochemical impedance spectroscopy experiments.

Finally, as shown in Figs. 2 and 3, both the hydrogen surface coverage removal and the oxide growth in acidic SC2 and neutral pure H_2O_2 were extremely slow as compared to the same processes occurring in SC1 solution. Such behaviour had already been pointed out in previous publications [11], and according to Niwano [29] 40% residual $Si\text{–}H_x$ bonds was observed even after a few hours, which was interpreted as an enhancement of the $Si\text{–}H_x$ stability in acidic media because of the hydrogen exchange with the solution. Moreover, the more compact and insulating structure of the generated oxide acts as a barrier to the transport of both reactants and ions through the layer This situation not only results in an extremely low oxidation rate, but necessarily promotes a lateral growth of the initial nuclei, i.e., a propagation of the oxide coverage proceeding by expansion of the islands generated during the initiation step [13].

5. Conclusion

The analysis by electrochemical impedance spectroscopy was very sensitive in revealing the dielectric behaviour of the oxide insulating layer at the surface of a silicon substrate, and more specifically, to the chemistry of the surface oxide, depending on its acido-basic properties. All facts were checked by various other complementary techniques such as ellipsometry and IR spectrometry. The growth of chemical oxides in peroxide mixtures was modelled by a mechanism involving the transport of species through the oxide layer corresponding to the conditions of the parabolic law, but complemented by a simultaneous dissolution process leading to a limiting constant thickness due to the appearance of a steady state regime. As a consequence it was possible to detect the solubility of Si chemical oxide both in alkaline and in acidic solutions on the nanoscopic scale always neglected in previous studies. It was thus possible to extract relevant parameters helpful for an optimization of the processing conditions to obtain a thin and uniform silicon oxide layer. We confirmed that chemical oxides grew growing uniformly and more rapidly in alkaline SC1 solutions. On the other hand, during the growth in acidic SC2 solutions, non oxidized regions were clearly detectable at room temperature, thus indicating a mechanism involving the spreading of oxide islands.

We have also pointed out that refining the IR-ATR results in the area of the Si–O–Si stretching vibrations allows the qualitative control of the uniformity and the structure of the oxide layer. One of the goal of the future cleaning treatments is to improve the atomic structure of the surface, which concerns both complete $Si\text{–}H_x$ removal and, at the same time, the possible control of the silicon oxide thickness on the scale of a few

Å. Moreover the surface structure of this oxide could be an important parameter for the build up of future multi-component high-k dielectric layers.

Acknowledgements

The authors acknowledge financial support of STMicroelectronics Co., and CEA/LETI for technical assistance.

References

[1] W. Kern, D.A. Puotinen, RCA Rev. (1970) 186.
[2] W. Kern (Ed.), Handbook of Semiconductor Wafer Cleaning Technology, Noyes Publications, New Jersey, 1993.
[3] S. Ojima, K. Kubo, M. Kato, M. Toda, T. Ohmi, J. Electrochem. Soc. 144 (1997) 1482.
[4] R. Sugino, Y. Okui, M. Shigeno, S. Ohkubo, T. Katasaki, T. Ito, J. Electrochem. Soc. 144 (1997) 3984.
[5] L.S. Woo, Jpn. J. Appl. Phys. 42 (2003) 5002.
[6] F. Tardif, T. Lardin, R. Novak, Solid State Phenomena 65/67 (1999) 19.
[7] B. Brar, G.D. Wilk, A.C. Seabaugh, Appl. Phys. Lett. 69 (1996) 2728.
[8] G. Gould, E.A. Irene, J. Electrochem. Soc. 136 (4) (1989) 1108.
[9] S. Adachi, K. Utani, Jpn. J. Appl. Phys. 32 (9A) (1993) L1189 (Part 2).
[10] D.-H. Eom, S.-Y. Kim, K.-K. Lee, K.-S. Kim, H.-S. Song, J.-G. Park, Proc. Electrochem. Soc. 36–99 (1999) 288.
[11] T. Ohmi, T. Isagawa, M. Kogure, T. Imaoka, J. Electrochem. Soc. 140 (1993) 804.
[12] H. Ogawa, N. Terada, K. Sugiyama, K. Moriki, N. Miyata, T. Aoyoma, R. Sugino, T. Ito, T. Hattori, Appl. Surf. Sci. 56–58 (1992) 836.
[13] Y. Sugita, S. Watanabe, Jpn. J. Appl. Phys. 37 (1998) 3272.
[14] H. Ogawa, K. Ishikawa, S. Fujimura, J. Electrochem. Soc. 143 (1996) 2995.
[15] N. Rochat, A. Chabli, F. Bertin, M. Olivier, C. Vergnaud, P. Mur, J. Appl. Phys. 91 (2002) 5029.
[16] Y. Sugita, S. Watanabe, N. Awaji, Jpn. J. Appl. Phys. Part 1 35 (1996) 5437.
[17] V. Bertagna, R. Erre, F. Rouelle, M. Chemla, S. Petitdidier, D. Lévy, Electrochim. Acta 47 (2001) 129.
[18] V. Bertagna, R. Erre, F. Rouelle, D. Lévy, S. Petitdidier, M. Chemla, J. Solid State Electrochem. 5 (2001) 306.
[19] V. Bertagna, F. Rouelle, M. Chemla, J. Appl. Electrochem. 27 (1997) 1179.
[20] Y.B. Wang, P. Han, Q. Chen, M. Willander, J. Appl. Phys. 82 (1997) 5868.
[21] F. Yano, A. Hiraoka, T. Itoga, K. Kanehori, Y. Mitsui, J. Vac. Sci. Technol. A 13 (1995) 2671.
[22] G.K. Celler, D.L. Barr, J.M. Rosamilla, Electrochem. Solid State Lett. 3 (2000) 47.
[23] D.W. Berreman, Phys. Rev. 130 (6) (1963) 2193.
[24] C. Wagner, K. Grunewald, Z. Phys. Chem. B 40 (1938) 455.
[25] B.E. Deal, A.S. Grove, J. Appl. Phys. 36 (1965) 3770.
[26] F. De Smedt, C. Vinkier, I. Cornelissen, S. De Gendt, M. Heyns, J. Electrochem. Soc. 147 (2000) 1124.
[27] F.P. Fehlner, N.F. Mott, Oxidation Met. 2 (1970) 59.
[28] S. Petitdidier, F. Guyader, K. Barla, D. Rouchon, N. Rochat, R. Erre, V. Bertagna, in: Society Proceedings, Cleaning Technology in Semiconductor Device Manufacturing VII, vol. 2001–2026, 2001.
[29] M. Niwano, Surf. Sci. 427–428 (1999) 199.